

Article

# LiDAR-Based Solar Mapping for Distributed Solar Plant Design and Grid Integration in San Antonio, Texas

Tuan B. Le <sup>1</sup>, Danial Kholdi <sup>1</sup>, Hongjie Xie <sup>2,\*</sup>, Bing Dong <sup>3</sup> and Rolando E. Vega <sup>1</sup>

<sup>1</sup> Texas Sustainable Energy Research Institute, University of Texas at San Antonio, One UTSA Circle, San Antonio, TX 78249, USA; lebaotuan@gmail.com (T.B.L.); danial.kholdi@gmail.com (D.K.); rolando.vega@utsa.edu (R.E.V.)

<sup>2</sup> Department of Geological Sciences, University of Texas at San Antonio, One UTSA Circle, San Antonio, TX 78249, USA

<sup>3</sup> Department of Mechanical Engineering, University of Texas at San Antonio, One UTSA Circle, San Antonio, TX 78249, USA; bing.dong@utsa.edu

\* Correspondence: hongjie.xie@utsa.edu; Tel.: +1-210-458-5445

Academic Editors: Richard Müller and Prasad S. Thenkabail

Received: 7 December 2015; Accepted: 11 March 2016; Published: 16 March 2016

**Abstract:** This study represents advancements in the state-of-the-art of the solar energy industry by leveraging LiDAR-based building characterization for city-wide, distributed solar photovoltaics, solar maps, highlighting the distribution of solar energy across the city of San Antonio. A methodology is implemented to systematically derive the tilt and azimuth angles of each rooftop and to quantify solar direct, diffuse, and global horizontal irradiance for hundreds of buildings in a LiDAR tile scale, by using already established methodologies that are typically only applied to a single location or building rooftop. The methodology enables the formulation of typical meteorological data, measured or forecasted time series of irradiances over distributed assets. A new concept on the subject of distributed solar plant (DSP) design is also introduced, by using the building rooftop tilt and azimuth angles, to strategically optimize the use and adoption of solar incentives according to the grid age and its vulnerabilities to solar variability in the neighborhoods. The method presented here shows that on an hourly basis DSP design could provide a 5% and 9% of net load capacity support per hour in the afternoon and morning times, respectively. Our results show that standard building rooftop tilt angles in the south Texas region has significant impact on the total amount of the energy over the course of a day, though its impact on the shapes of the daily energy profile is relatively insignificant when compared to the azimuth angle. Building surfaces' azimuth angle is the most important factor to determine the shape of daily energy profile and its peak location within a day. The methodology developed in this study can be employed to study the potential solar energy in other regions and to match the design of distributed solar plants to the capacity needs on specified distribution grids.

**Keywords:** LiDAR; renewable energy; solar mapping; distributed solar plant; San Antonio; Texas

---

## 1. Introduction

The concept of solar energy estimation under alternative scenarios of urban morphology has been widely studied and developed [1–3]. However, using Light Detection and Ranging (LiDAR) technology to characterize the morphology of a large area with very high resolution on surface orientations of buildings and to quantify potential solar energy as well as to support distributed residential solar plant design is a relatively new application. Higher accuracies in building 3D objects obtained from LiDAR (comparing to the traditional elevation and terrain models) allow potential solar energy calculation becomes more reliable [4]. This paper reports the results of a case study in San Antonio, Texas, aimed

at developing (1) a systematic approach for 3D solar mapping and (2) a new concept in distributed solar plant design. A distributed solar plant refers to the collective contribution of individual solar photovoltaic (PV) installations on buildings located in a specific electrical distribution grid or district.

LiDAR is a laser scanning system that utilizes laser technology to measure the distance from a sensor to objects. Airborne LiDAR sensor sends laser beams towards the ground and records the reflected beams for the intensity and time traveled. Objects on the ground are represented by many points which provide accurate three-dimensional locations. These points combine together to form point clouds that go beyond the bare earth Digital Elevation Models (DEM) by producing very high resolution of the Digital Surface Models (DSM) [5–7].

LiDAR data processing is an important task, because most of the end users, including engineers, researchers, planners, *etc.* are interested in feature classes, such as buildings, trees, roads, bridges, power lines, that should be already extracted and readily available for applications [8]. However, converting LiDAR point clouds to feature classes is not a simple process since it should consider not only the points' positions and elevations but also other coded attributes such as intensity, return number or numbers of return [8]. There usually is a correspondence between the object's characteristics, type of material and the return or intensity value. Within the scope of this study, we are focusing on generating building footprints and rooftops from LiDAR point clouds. These features will be utilized to serve distributed solar plan design and grid integration study in San Antonio area.

There are two main approaches toward extracting features from LiDAR data. In the first approach, the aerial images are used as masks for extracting features from the LiDAR data. For example, Liu *et al.* [9] proposed an approach in which both the LiDAR data and the aerial images are respectively preprocessed and matched using the affine transformation model. The second approach, which is more common, starts directly with the raw LiDAR data, trying to divide points into different classes (as bare earth, buildings, trees, *etc.*) in order to create the shape file database of the features. The very basis of the second approach is to extract the bare ground layer from the point clouds, leaving all other points including buildings footprints, vegetation, water, *etc.* Thus, the next step of the approach is separating buildings and vegetation (specifically trees) based on the values of return and return intensity. The resulting two-dimensional data base is then turned into three-dimensional models using information such as the minimum and maximum elevations of every surface (showing the flat or pitched roofs), coordinates of the buildings' footprints vertices, their area, *etc.* [10,11]. This approach is built in the ENVI LiDAR extension [12] and is used in this study.

Along with the popularization of LiDAR applications, GIS-based solar calculation and mapping has also been strongly developed using different algorithms such as the Masters' algorithm, American Society of Heating, Refrigerating and Air-Conditioning Engineers (ASHRAE) algorithm, System Advisor Model (SAM) algorithms [13–15]. Thus, computer software and tools have also been developed to bring these algorithms to end-users in a friendly way, such as Pysolar library (available at [pysolar.org](http://pysolar.org)), REST2 model [16], and PVMapper Site Designer (PVMSD) [17].

Pysolar is an online library of Python codes that implements the Masters' algorithm for solar irradiation calculation. Pysolar also uses an algorithm developed by the National Renewable Energy Laboratory (NREL) for solar position calculation in its performance [18]. The Masters' algorithm is a set of fairly straightforward equations that calculate the Sun's location in the sky at a specific time of a specific day and the potential solar irradiance in a clear sky condition as well as the irradiance reaching a horizontal or inclined surface on the ground. The Masters' algorithm uses the early version of the ASHRAE algorithm (version 1993) for solar irradiation calculation as several ASHRAE parameters are used in Master's equations such as optical depth, apparent extraterrestrial flux, and sky diffuse factor. In comparison with ASHRAE algorithm, the Masters' algorithm equations are simpler.

REST2 model, developed by a consulting company [16], is based on the ASHRAE solar calculation algorithm. Literature review indicates that ASHRAE algorithm is applied more popularly than Masters' algorithm in solar calculation study [19–23]. The latest version of ASHRAE algorithm is evaluated to be very reliable and can generate solar irradiance estimations with high accuracies, especially through

the performance of the latest version of the REST2 model [24]. However, REST2 model is not suitable for solar mapping and distributed solar plant design in San Antonio because the model is neither GIS-oriented nor open-source. Using ASHRAE algorithm requires a development of a computer application that can well integrated into GIS platforms.

PVMSD is one of the newest tools for solar calculation and mapping. The solar calculation model used in PVMSD is the SAM, developed by NREL [15]. The SAM Simulation Core (SSC) Software Development Kit (SDK) provided by NREL was used to design PVMSD [17]. PVMSD is open-source and advanced but there are limitations. For example, it only accepts KML format input files; modeling buildings in PVMSD does not consider the tilt and azimuth of rooftops surfaces which significantly affects solar irradiance estimation; PVMSD only allows performing irradiance calculation on one rooftop at a time which is inapplicable to multiple neighborhoods computation; and lastly, PVMSD does not provide the ability to select and deselect specific rooftops to run the model under alternative scenarios.

The analysis of the latest approaches in solar calculation leads to the decision of adopting the **ASHRAE algorithm for solar calculation** in this study. It also suggests that it is necessary to develop a new computer application that is GIS-oriented and can implement solar irradiance estimation based on the ASHRAE algorithm for large and multiple neighborhoods.

The purpose of this study is to develop a systematic approach to quantify solar irradiance components (direct, diffuse and ground-reflected irradiances) and potential solar energy at regional (citywide) and residential (neighborhood) level based on 3D building rooftops generated from LiDAR point clouds. Solar calculation and mapping tasks are performed through GIS-based computer applications developed during this study using the established theoretical methodology by ASHRAE. This study also examines building rooftop tilt and azimuth angles for distributed solar plant (DSP) design purposes through alternative rooftop selection scenarios. This information can be used strategically to optimize the use and adoption of solar incentives according to the grid age and its vulnerabilities to solar variability in the neighborhoods by adopting the rooftop surfaces that make a better contribution to grid asset life extension and/or smarter inverter controls.

## 2. Data and Methodology

### 2.1. LiDAR Data

LiDAR data for the San Antonio area were acquired by the Texas Natural Resources Information System (TNRIS). The data were collected in August, October, December 2010 and January 2011 with high spatial resolution of 50 cm and 95% accuracy as compared with the 39 survey checkpoints [25]. There are 458 LiDAR tiles (in a quarter-quarter-quad system) in LAS 1.2 format that cover approximately 4808.5 km<sup>2</sup> in and surrounding Bexar County (Figure 1). Each tile covers an area of approximately 3.03 km × 3.47 km.

LiDAR data were geo-referenced using the horizontal and vertical datum of North American Datum of 1983 (NAD83), the projection of Universal Transverse Mercator (UTM) for Zone 14 North, and horizontal and vertical units of meters. Each LiDAR point holds many attributes beside its X, Y coordinates and elevations, such as classification, intensity, return number, number of returns, flight line, edge of flight line, scan direction, scan angle, and GPS time. **Important attributes of each LiDAR point are classification, intensity, and number of returns** and are used to identify objects' characteristics and geometries.

Elevation (Z value) of LiDAR point is an important attribute when processing the data. Elevation is expressed in meters above the mean sea level. Elevation is also useful to calculate the above ground level (AGL) of objects by subtracting the corresponding DEM value from DSM. AGL is actually the height from the ground that involves into the geometry extraction process from the point clouds.

Other important attributes of LiDAR data such as density, intensity and return number are well explained by Gatziolis and Andersen [26]. The LiDAR dataset for San Antonio area in this study

has average density from 6.75 points/m<sup>2</sup> in heavily developed areas to 1.81 points/m<sup>2</sup> in opened space areas with just ground points. With this density, the point clouds have no more than 1.6 feet point spacing, which meets the Level of Detail (LOD) 2 and is qualified to produce good accuracy of rooftop extraction. Density helps visually recognizing rooftop surfaces of commercial buildings and residential houses, however, converting them to geometric feature classes is a complex process. Intensity attribute is significantly meaningful in classifying point clouds and also a valuable aid in detecting and extracting features. Going beyond the popular application of intensity values in detecting building geometries and materials [27–29], these LiDAR attributes could also be used to detect different species of vegetation [30]. The intensity values in LiDAR dataset for San Antonio range from 0 to 16,829 with high intensities represent high reflectance materials. More than 70% of LiDAR points have intensity below 80 with the average intensity of the entire point clouds varies from 20 to 30 among the LiDAR tiles. There are overlapping between classes. This makes it difficult to classify objects just based on intensity values alone.

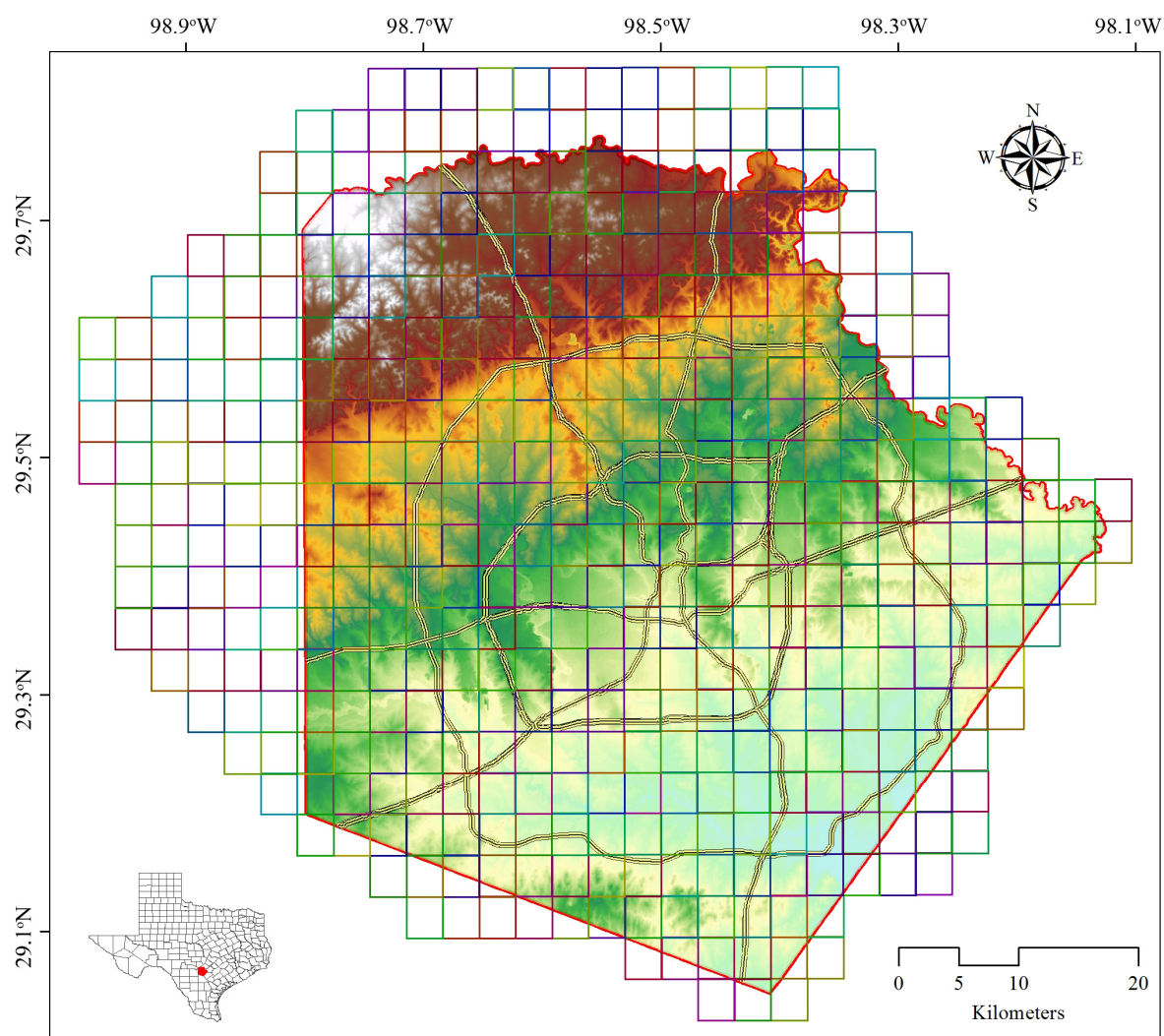


**Figure 1.** 458 LiDAR tiles over the San Antonio (Bexar County), Texas area, overlaying with major highways.

Besides the above-mentioned attributes of each LiDAR point, a set of numerical codes from 1 to 13 were also assigned to each LiDAR point. Only 7 of them are seen in this study due to the characteristics of measured data in San Antonio area, including 1 (Unclassified points), 2 (Bare earth

points), 6 (Building points), 7 (Low points or noise points), 9 (Water points), 12 (Overlap points) and 13 (Bridge or culvert points).

## 2.2. Feature Extraction

Point clouds processing for feature extraction takes into account all LiDAR attributes and classification codes mentioned above. Data-driven approach is applied for automatic feature reconstruction. This approach is appropriate for high-density point clouds and is well documented in previous studies [31–33]. Feature identification can be performed on an entire point cloud tile or a user-defined subset of a scene, providing users with accurate information in a fraction of the time. Features that can be extracted include trees (X, Y, Z, H (height), R (canopy radius)), power line vectors, power poles (X, Y, Z, H), power line attachments (X, Y, Z), Digital Surface Model (Grid, TIN), Digital Elevation Models, classified point cloud, ground contours, building roof face vectors, building perimeter vectors, and point density and coverage analysis. Figure 2 shows a sample 2D building footprints produced for an area within the University of Texas at San Antonio (UTSA) main campus.



**Figure 2.** Building footprints of University of Texas San Antonio (UTSA) campus generated using ENVI LiDAR extension.

## 2.3. Tilt and Azimuth Angles Extraction

Tilt and azimuth angles of each rooftop surface are calculated based on a simple process described in Figure 3. Points chosen from each rooftop hold the same ID in their attributes to help identify which rooftop they belong to. Figure 3 also provides the linear algebra equations that used to calculate tilt and azimuth angles from vertices.

Steps in this process can be briefly described as follows: (1) select three points (named A, B, and C) with the same original FID; (2) calculate the vectors AB and AC using the coordinates of the three selected points; (3) calculate the cross product of vectors AB and AC, calling it N (calculating the normal vector to the rooftop); (4) calculate the title angle between the normal vector N and the unit

vector K (0,0,1); and (5) calculate the azimuth angle between the normal vector N and the unit vector J(0,1,0). Figure 4 shows an example of tilt and azimuth angles for a small neighborhood.

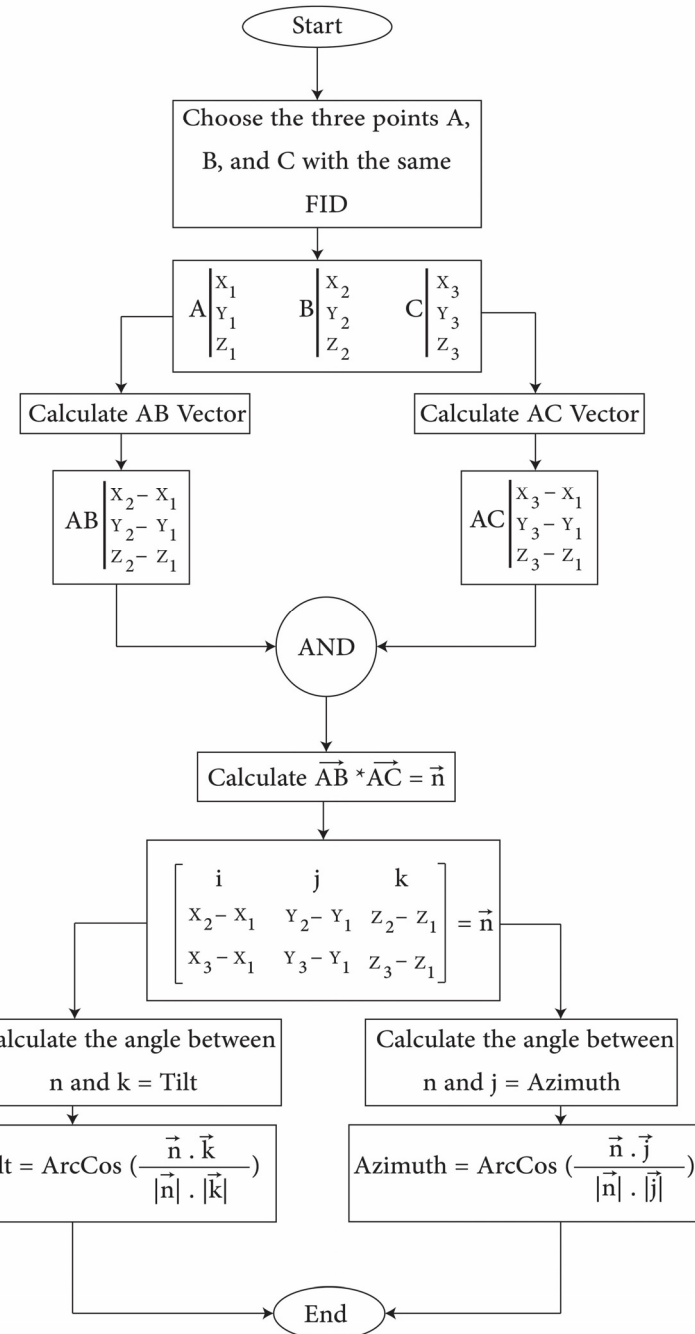


**Figure 3.** Flowchart of tilt and azimuth angles calculation [34].

#### 2.4. Solar Irradiance Calculation

Potential solar energy for San Antonio area is calculated by a computer program developed in this study using Python language and based on the ASHRAE algorithm. This program is designed to calculate direct, diffuse, ground-reflected as well as global horizontal irradiance on multiple surfaces for a specific time instant. For results here, a 1-h time interval has been chosen to calculate irradiances. The program can also run for 24 h of a selected date or hourly for 365 days of a year depending on the interest of users. Its input file is in CSV (comma delimited) format that contains 7 columns. Column 1

is the IDs of the roof surfaces, at one ID per roof surface; column 2 is the areas of each surface in square meters; columns 3 and 4 are the X and Y coordinates of the center point of each surface in meter, respectively; column 5 is the elevation of the center point of each surface; column 6 is the tilt and column 7 is the azimuth of each surface. This input file is exported from the processed building shapefile mentioned in Sections 2.2 and 2.3. The program runs through all the surfaces contained in the list and calculate the irradiance for each of them for the defined timing. The program's output is a CSV file in tabular format that stores all the irradiance estimations of each surface for all selected hours.

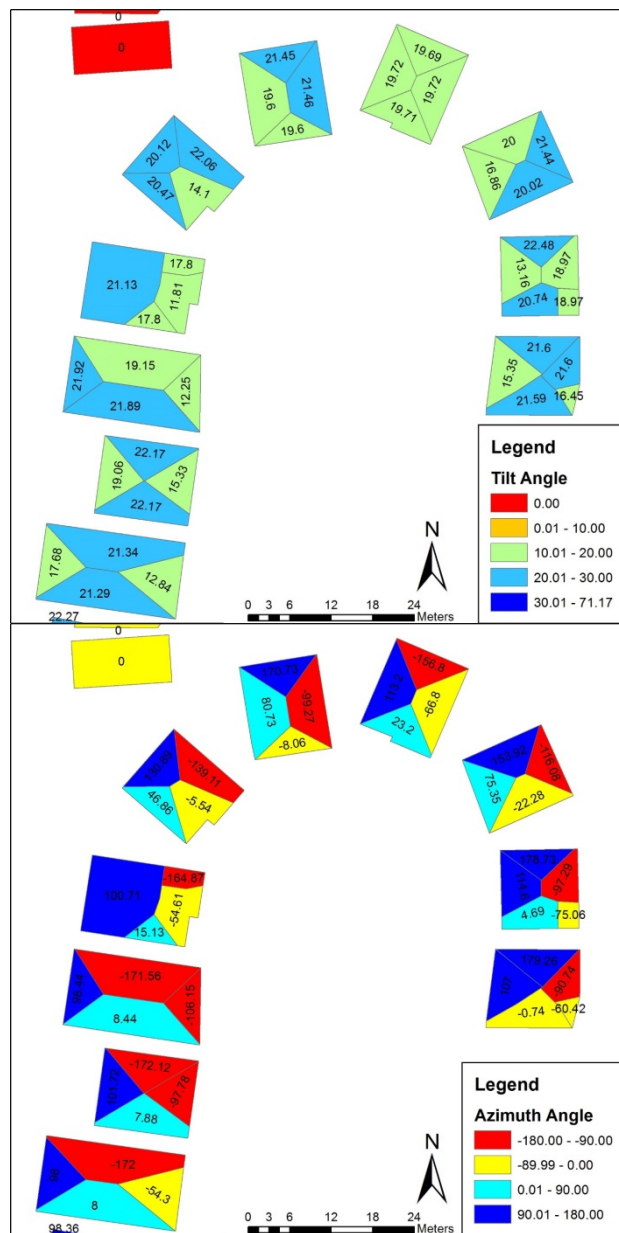


**Figure 4.** Map showing the tilt and azimuth angles generated for a sample area (azimuth angle adopts the ASHRAE tradition where  $0^{\circ}$  to south,  $180^{\circ}$  to north, negative to east, and positive to west).

The total irradiance of each surface is the sum of three components: direct, diffuse and ground-reflected irradiances. Each of the components is a function of its normal and horizontal irradiance and the angle of incidence to the surface. These components are calculated separately.

$$E_{t,b} = E_b \cos \theta [14]$$

$$Et,d = Ed \max(0.45, 0.55 + 0.437 \cos \theta + 0.313 \cos^2 \theta) [14]$$

$$Et,r = (Eb \sin \beta + Ed) \rho g (1 - \cos \sum) / 2 [14]$$

where  $Et,b$ ,  $Et,d$ , and  $Et,r$  are direct, diffuse and ground-reflected irradiances on a surface, respectively;  $Eb$  and  $Ed$  are direct normal and diffuse horizontal irradiances, respectively;  $\theta$  is the angle of incidence of the surface;  $\beta$  is solar altitude angle;  $\sum$  is surface tilt angle; and  $\rho g$  is ground reflectance.

$Eb$  and  $Ed$  are portions of the extraterrestrial normal irradiance that is approximately constant for the same Julian date among the years. The calculation of  $Eb$  and  $Ed$  are strongly affected by the optical depths and air mass (a function of solar altitude) [14]. In our program, the optical depths are computed from the Typical Meteorological Year (TMY) 3 dataset for San Antonio collected at the San Antonio International Airport. This dataset includes real measurements of hourly extraterrestrial radiation normal to the sun (ETRN), hourly extraterrestrial radiation on a horizontal surface (ETR), hourly direct normal irradiance (DNI) and hourly diffuse horizontal irradiance (DHI) that serve the Beer-Lambert law to estimate the direct and diffuse atmospheric optical depth. Briefly, the Beer-Lambert law in the atmosphere is represented as:  $I = Io \exp(-m\tau)$ ; where  $Io$  and  $I$  are the intensity of incident and transmitted radiation, respectively;  $m$  is air mass and  $\tau$  is optical depth. When calculating direct optical depth, ETRN and DNI are used as  $Io$  and  $I$ , respectively; and for diffuse optical depth calculation, ETR and DHI are used instead.

## 2.5. Rooftop Selection Approaches

Distributed solar power plants (DSPPs) that are designed incorporating rooftop directionality knowledge from data sources such as LiDAR can contribute to the optimization of power reserve margins by introducing a responsive time-dependent smart rooftop PV engagement functionality. Differing from the “single-house” solution designed with the self-proclaimed needs of the home owner that would lead to a time-noon-synchronized aggregated peak of maximum generation of power that can be detrimental or not as useful to the electric grid, the DSPPs can (1) extend the life of the distribution grid which translates to less expenses to the utility; (2) not have to over design the upgraded grid; and (3) minimize the electrical losses of the power plants that the utility have to engage (and that often can be very far from the homes) to supply the power needs and are able to better supply the community energy needs by the homes in those same communities with the concept of distributed solar plant design. In Texas, for example, the Electric Reliability Council of Texas (ERCOT) has brought national attention because projections of the supply and demand of electricity in the State indicate that the reserves will not satisfy the national NERC standard of 13.75%, but rather it is predicted to fall below this level by 2019 to as low as 7.3% by 2023 [35].

Two main approaches for rooftop selection, **orientation-based approach and energy-based approach**, are developed in this study. The orientation-based approach tends to select the rooftops through a set of conditions. For instance, selected rooftops must face south orientation with the bounds of west and east orientations, having surface tilts from 18 degrees to 27 degrees, and having an area of at least  $10 \text{ m}^2$ . This set of conditions can be expressed in the computer program as ( $\text{Azimuth} \geq -90$ ) AND ( $\text{Azimuth} \leq 90$ ) AND ( $\text{Tilt} \geq 18$ ) AND ( $\text{Tilt} \leq 27$ ) AND ( $\text{Area} \geq 10$ ). This set of conditions can be easily modified to meet a specific requirement of distributed solar plant design for an area. The advantage of this approach is in finding the optimal rooftop surfaces that potentially produce the maximum solar energy and also suitable for PV installation. However, the orientation-based approach cannot provide an estimation of targeting amount of energy prior to rooftop selection.

Differing from the orientation-based approach, the energy-based approach selects the rooftops surfaces based on the total amount of energy that are potentially required to produce. The total energy of each rooftop surface on the representative days, such as on the 21st of each month, is calculated and then sorted descending. rooftops are then selected top down until the total energy of the selected rooftops is equal to the expected value. This process is repeated on various days throughout the year to find the common selected rooftop surfaces. These common rooftops are considered as the optimal

surfaces for the distributed solar plant of the area. Similarly to the orientation-based approach, the energy-based approach also has its pros and cons. It can limit the total potential energy to a specific value that we expect but the number of selected rooftops for PV installation to meet that value can vary. In addition, the number of common rooftops among the calculated days can possibly be small or zero in some areas. In this case, distributed solar plant design will have to face such limitations if only this design-intelligence is not systematically used with other distributed enabled technologies.

### 3. Results of Solar Mapping

#### 3.1. DEM-Based Irradiance Analysis

Solar mapping based on the calculation of developed program is performed at both the regional scale (using 10 m DEM of Bexar County) and the neighborhood scale (using rooftop geometries of each LiDAR tile). The approach, however, is the same for both applications. Estimated irradiance values in the output file are transferred into GIS as the attribute table of equivalent feature class by using the ID of each record. For the DEM-based solar mapping, the feature class is the TIN surfaces generated from the 10 m DEM and for the LiDAR-based solar mapping, the feature class is the rooftop surfaces of the buildings.

DEM-based solar mapping starts with the conversion from 10 m DEM to TIN which is a network of triangle surfaces that represent the ground surface. TIN is then converted into a feature class of multiple triangle features (Figure 5). Each triangle is defined by its central X and Y coordinates, central elevation, tilt and azimuth. Calculated irradiances for each triangle are transferred into their attribute table by relating to the program's output tabular file through the triangle IDs. Irradiance values can then be displayed as a map. A demonstration of solar mapping on 21 July at 10 o'clock in the morning (Figure 6) indicates that hourly direct irradiance on the ground surface potentially ranges from 200 to 400 W/m<sup>2</sup> approximately, with red indicating high potential solar irradiance and green for low potential solar irradiance. On the surfaces that are facing east, direct irradiance is mostly above 350 W/m<sup>2</sup>. Inversely, surfaces that are facing west receive direct irradiances that are below 350 W/m<sup>2</sup>. DEM-based solar maps are available for 3 irradiance components (direct, diffuse and ground-reflected) as well as for global horizontal irradiance hourly of 365 days of a year.

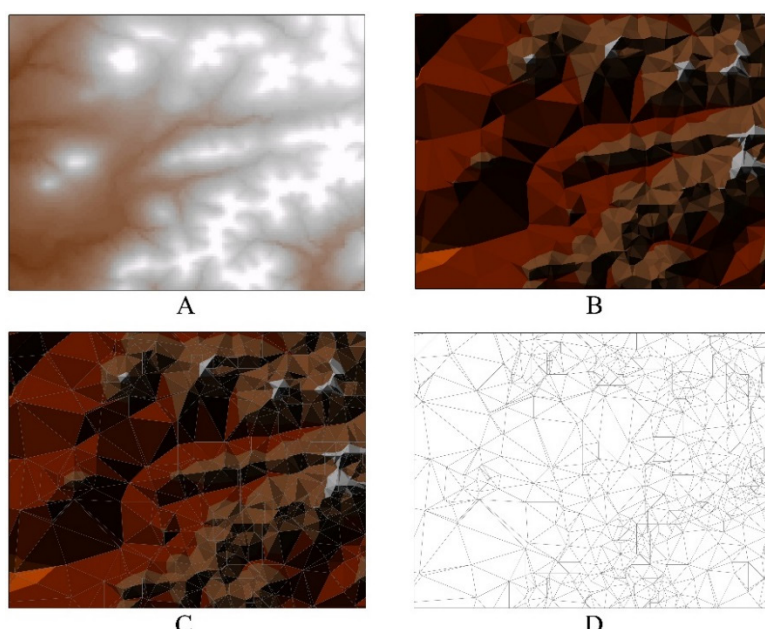


**Figure 5.** DEM (A) converts to TIN (B), TIN with edges (C), and to triangle features (D).

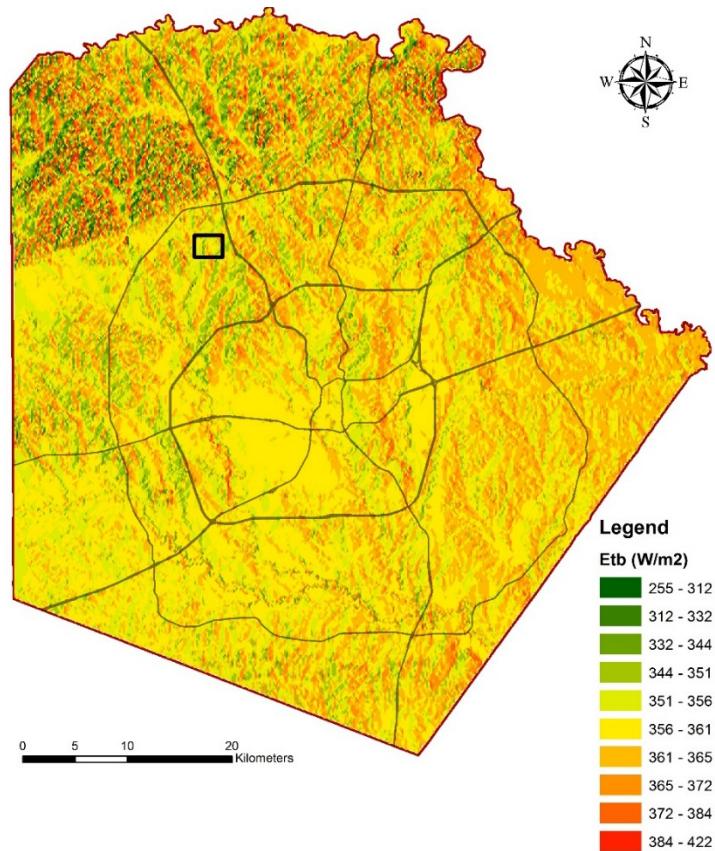


**Figure 6.** DEM-based solar map of San Antonio (Bexar County) on 21 July at 10:00 a.m., overlaying with major highways (black lines) of San Antonio and the neighborhood area (black rectangular box) for rooftop irradiance analysis (in Figure 7).

### 3.2. Building-Level Rooftop Irradiance Analysis

A similar process is also applied for building-level solar mapping. Instead of inputting the defined triangle features to our computer program, geometries of building rooftops are used. LiDAR-based solar map processing is performed on each building rooftop (of a LiDAR tile) at a time. This LiDAR-based type of rooftop modeling is known as the best optional for residential areas [36]. Solar maps at neighborhood scale for the entire San Antonio area can be calculated for every hour of 365 days of the year. Figure 7 is the illustration of the hourly direct irradiance on 21 July in the morning and afternoon on every rooftop surfaces of a neighborhood near the UTSA Main Campus, Northwest San Antonio (seen in Figure 6). These calculations do not take into account shading factor as the program is designed for clear-sky condition. Clearly, the higher direct irradiances in the morning are those roofs facing east (Figure 7A) and in the afternoon are those roofs facing west (Figure 7B).

Comparing solar calculation using DEM (Figure 6) and LiDAR-derived roof surfaces (Figure 7) for the same morning time (10:00 a.m. on 21 July) shows relatively matching maximum potential solar irradiance, although as expected there are deviations (in this case of approximately 40 W/m<sup>2</sup>). DEM maps are a general view of the terrain inclination angles and building rooftop surfaces indeed have deviations around this and fluctuating around a leveled horizontal plane as opposed to the ground surface plane of array (POA). Direct irradiances in the afternoon (3 p.m.) estimated are much higher with maximum values reaching above 850 W/m<sup>2</sup> for 21 July. These values of direct solar irradiance are within the expected range for this time of day. However, these estimates and in particular the diffuse solar irradiance component should be verified by actual measurements accounting for cloud shading and aerosol effects.

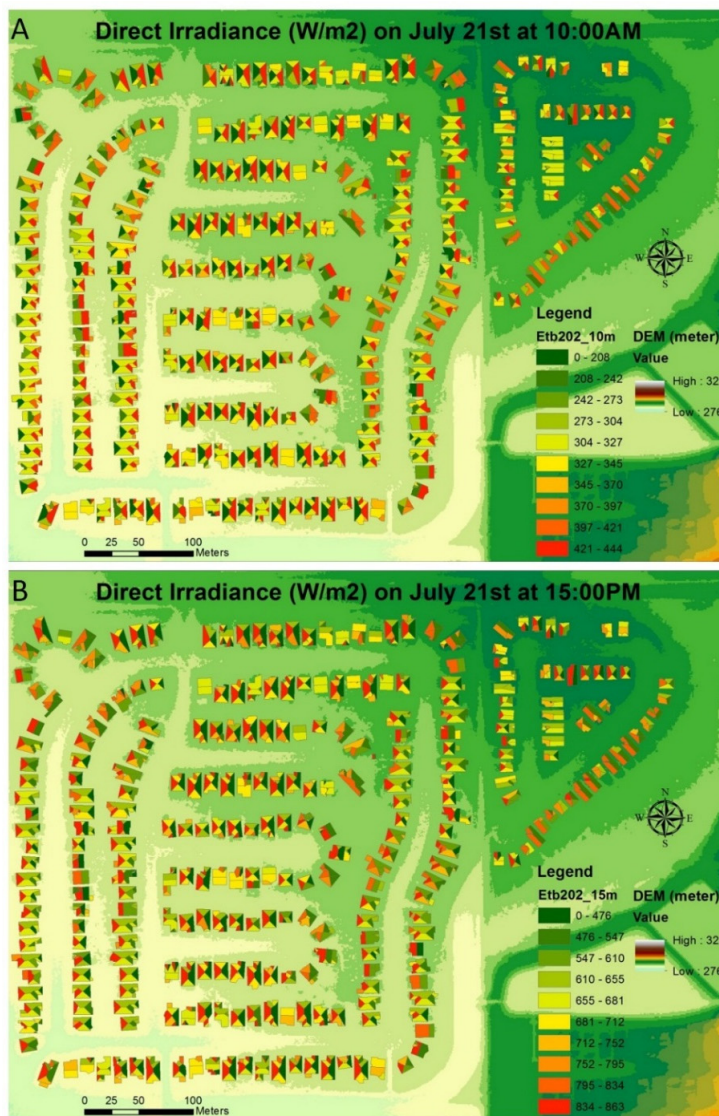


**Figure 7.** LiDAR-based solar map of a neighborhood in San Antonio on 21 July at 10:00 a.m. (A) 15:00 p.m. (B).

### 3.3. Potential Power Calculation

Total daily solar power can also be computed for each LiDAR tile. This is the potential solar power that can be produced from all rooftop surfaces available within a LiDAR tile. Figure 8 represents the power estimations for the 21st day (only accounting the day-time hours) of each month in one LiDAR tile. Very large amounts of potential solar power (in MW) are estimated; however, these calculations are based on an assumption of unobstructed building condition. Other factors, such as cloud, shading effect, PV efficiency, percentage of selected rooftops, need to be taken into account to gain more practical estimations when considering distributed solar plant design—as will be shown in Section 4. In fact, these influential factors considerably affect the potential of rooftop surfaces in producing solar power [37]; so future work will include an enhancement of ray tracing algorithms to explicitly account for tree and building shading interference on each site.

The city-wide distributed solar energy potential map can be produced by using the DEM-based solar mapping approach as shown in Figure 9, an example of 4 dates (21 March, 21 June, 21 September, and 21 December) and 3 times (9, 13, and 16 h) of each date. The accumulation of these 12 solar power estimates shows the pockets of higher and lower energy potential in San Antonio.

The four dates chosen represent the range of earth-sun relative positioning during an entire year (following the extreme solstice and equinox locations), thus providing an excellent metric of relative annual energy potential. The quantitative values should not be used for economic analysis but the spatial distribution of high and low energy density areas is as representative as if the analysis is rendered for all the 8766 h in a year.

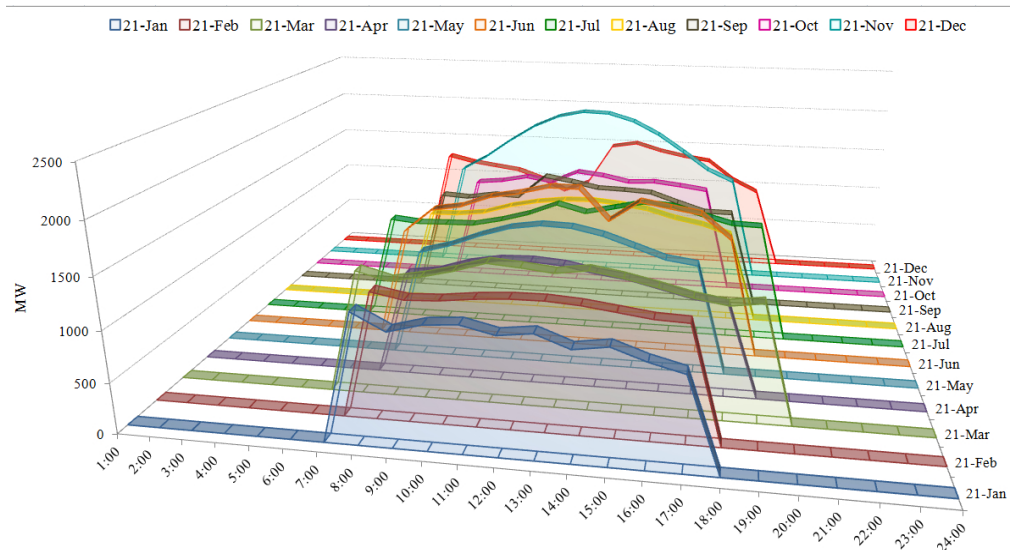


**Figure 8.** Total power estimation (in MW) be potentially produced from all rooftops within one LiDAR tile that covers the UTSA main campus (calculation for the 21st of each month).

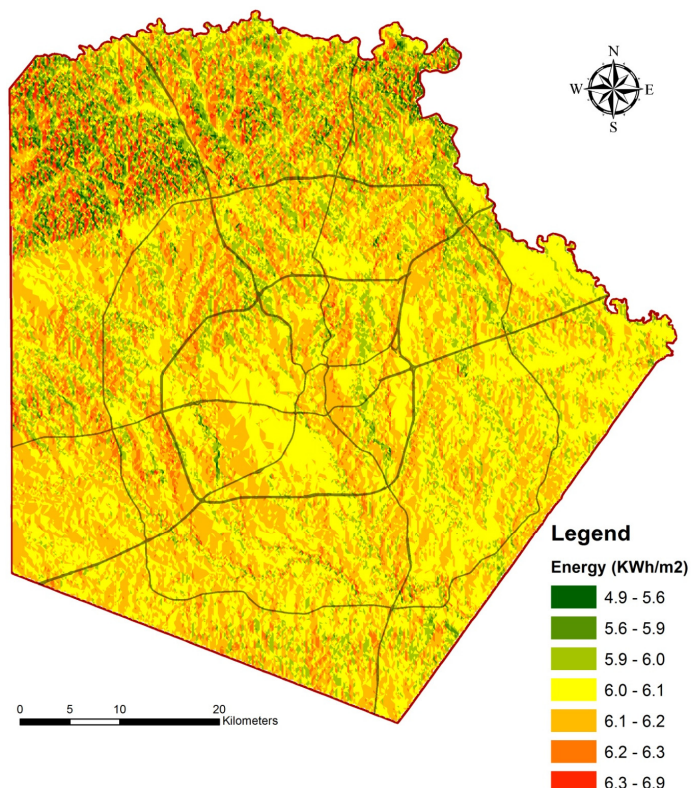


**Figure 9.** Distributed solar energy potential in Bexar County (calculated from direct irradiance on 21 March, 21 June, 23 September and 22 December at morning, noon and afternoon hours of each day).

## 4. Distributed Solar Plant Design

### 4.1. Assessment of Potential Rooftops

The selection of potential rooftop surfaces that contribute to the distributed solar plant is significantly based on their distribution of tilt and azimuth angles. Sarralde *et al.* [3] recently presents the advantages of studying urban morphology (including building orientation/tilt) in increasing the potential harvest solar energy. Huang *et al.* [38] also recognized significant influence of urban morphology that is characterized by building densities and rooftop structures on solar irradiance. Therefore, analyzing urban morphology in general and tilt and azimuth angles in particular is an important task to identify potential and suitable rooftops for distributed solar plant. A distributed solar plant refers to the collective contribution of individual solar photovoltaic installations on buildings located in a specific electrical distribution grid or district. In addition, when designing a distributed solar plant, the target producing energy should be pre-defined, so that rooftop selection can take into account not only surface orientation but also target energy amount. This section describes an experiment of smart rooftop selection and distributed solar plant design in an area in the northwestern San Antonio covered by a LiDAR tile. Most significantly in this section is to see how distributed solar power can flatten out over the course of the day much like when solar trackers are installed in utility-scale solar plants.

The distribution of rooftop azimuth angles in the selected area of the LiDAR tile is represented in Figure 10. Surprisingly, surface azimuth angles of 0, 90, −190 and 180 degrees count the most of rooftop surfaces. Unlike in meteorology, 0 degree represents facing south surfaces, −90 degrees and 90 degrees represent facing east and west surfaces respectively, and 180 degree or −180 degrees represents facing north surfaces according to ASHRAE [14]. In fact, in the northern hemisphere, surfaces facing south receive more solar irradiance because the earth's inclination and relative orbiting around the sun make the solar position on the sky to be off towards the south by as much as the latitude amount of the site during the day. For that reason, azimuths facing south are approximately the optimal orientation for solar energy production. The selection of only facing south rooftop surfaces may not ensure the expected amount of energy for an area. Therefore, rooftops facing east and west can also be considered to be selected. In other words, rooftop surfaces whose azimuths range from −90 degrees to 90 degrees would be the targets for more economically favorable rooftop selection for the consideration of distributed solar plant design.

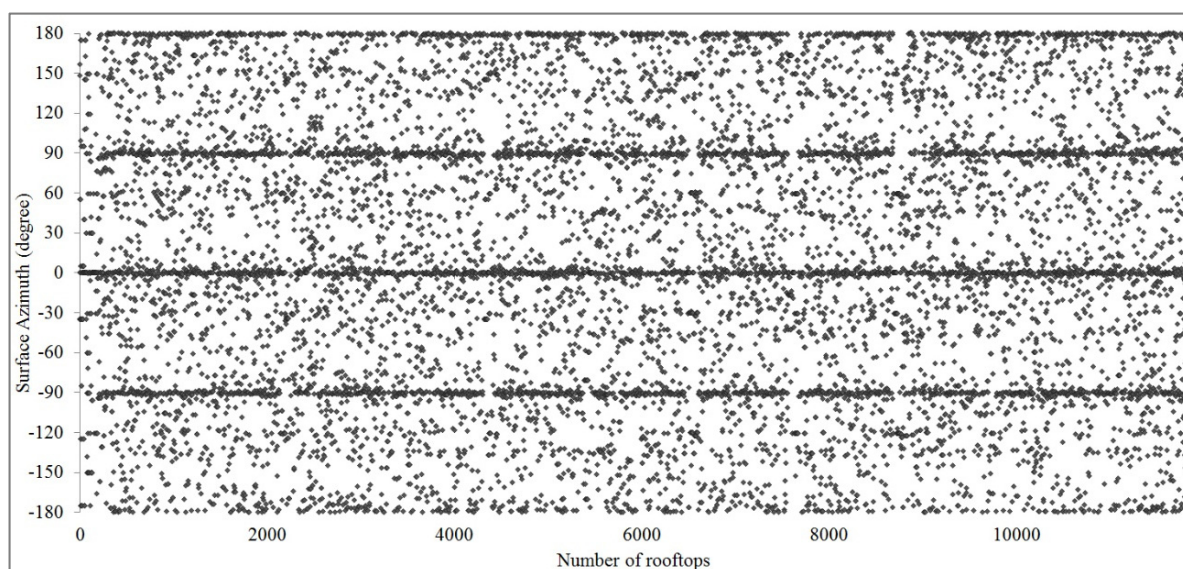


**Figure 10.** The distribution of surface azimuth of all rooftops from a LiDAR tile.

The distribution of surface tilt is also examined and represented in Figure 11. Rooftop surfaces of buildings, with the majority of residential houses in the LiDAR tile area have the tilt mostly from 18 to 27 degrees. Commercial building's rooftops usually have surface tilt below 2 degrees and those can be seen in Figure 11. When designing a distributed solar plant for a neighborhood, target surfaces are the residential houses' roofs. For that reason, rooftop selection in the next section focuses on 18–27 degrees range of surface tilts.

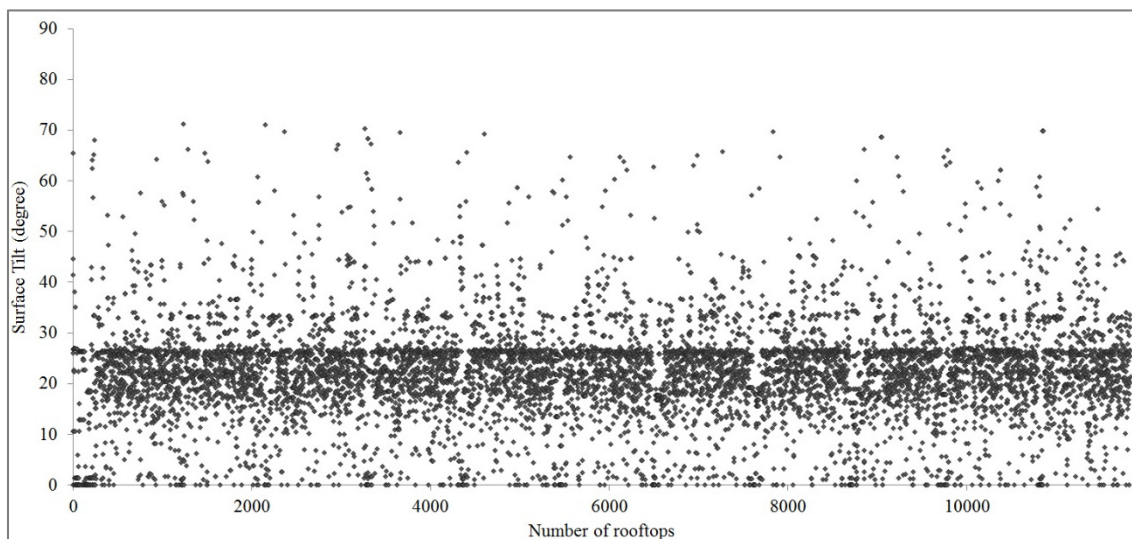


**Figure 11.** The distribution of surface tilt of all rooftops from a LiDAR tile.

#### 4.2. Electric Load, DSP Rooftop Selection and Model Scenarios

Figure 12 shows an example of distributed solar plant design using the orientation-based approach, for a small neighborhood located in the northwest of San Antonio. There is a total of 2226 rooftop surfaces in this neighborhood with their surface azimuth uniformly distributed around four major azimuths (north, east, south, and west). This accounts for 463 residential homes and two office buildings. The total community residential load was calculated using a U.S. Department of Energy dataset that contains hourly load profile data for commercial building types (based off the DOE Commercial Reference Building Models) and residential buildings (based off the Building America House Simulation Protocols). The dataset also uses the Residential Energy Consumption Survey (RECS) for statistical references of building types by location. Hourly load profiles are available for all TMY3 locations in the United States. We have adopted a community with 70% average, 9% with low and 21% with high energy consumption models located in San Antonio, Texas. We have the commercial building models corresponding to Medium Size Office. The examination of potential solar energy from this selected area is performed under six alternative scenarios. Each scenario defines specific thresholds of surface tilts and azimuths for rooftop selection; then, solar energy from selected rooftops is calculated to generate the energy curve for a day. We have assumed a premium module type with 18% efficiency, a fixed open rack array and losses of 14% as presented in Table 1 and discussed in Dobos [39]. We have assumed to use a ground coverage ratio (GCR) of 0.2 to account for the general adoption of rooftop solar in the neighborhoods and an inverter efficiency of 96%. Figure 13 shows an example of the daily load and solar power profiles for the date of 21 July under the six rooftop selection scenarios. These scenarios show what is the DSP generation penetration into the grid on an hourly basis, and it also shows what is the total power generation response as different rooftop orientations are engaged. We have calculated the average load over the daylight hours to focus our attention on the overall magnitude of daily net load capacity support provided with better DSP design. We measure the magnitude of net load capacity support by determining the slope of the DSP generation profile

(*i.e.*, with units of kW per hour) and divide this by the average load during the day resulting in the percentage (%) of the net load that can be absorbed over one-hour by an optimized DSP design. In the future, shorter time intervals should be studied accounting for the spatial dispersion of the solar irradiance on neighborhoods to ascertain shorter ramp-down and ramp-up events and how the DSP can support the grid with ramp-event smoothening.

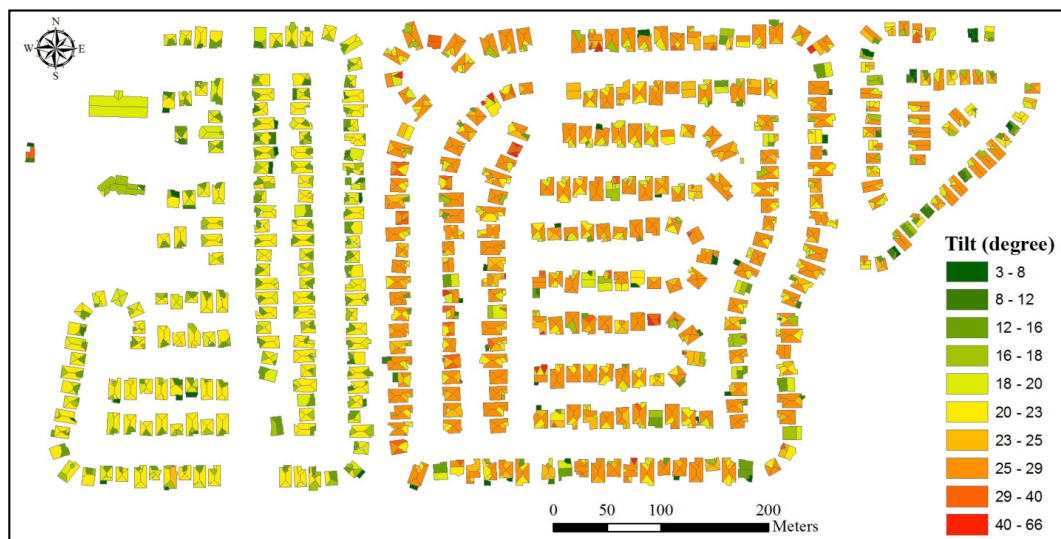


**Figure 12.** Selected neighborhood for the demonstration of distributed solar plant design.

**Table 1.** System losses.

Loss Mechanism	System Losses
Soiling	2%
Shading	3%
Snow	0%
Mismatch	2%
Wiring	2%
AC Wiring	0%
Connections	1%
Light-induced degradation	2%
Nameplate rating	1%
Age	0%
Availability	3%
<b>Total Losses</b>	<b>14%</b>

As can be seen in scenarios A and B in Figure 13, when the rooftop surfaces facing west are selected, the generation power profile has an increasing generation amount throughout the day matching more closely the electrical load with generation peaks around noon and hour 3–4 p.m. These two peaks can be justified with the distribution of westerly rooftop surfaces that have a southerly component and those that more strictly west or perhaps with a northerly component. The surface tilt does not significantly affect these shapes, although it changes the magnitude of potential solar power due to different amount of rooftops selected. With the threshold of 1–10 degrees tilt applied in scenarios A and C, only a small numbers of rooftops are selected corresponding to commercial buildings with flat or small tilt angles rooftops. Commercial buildings in the selected LiDAR tile represent a very small set and therefore their contribution to DSP design for net load capacity support s negligible. However, the power profiles in scenario B have larger magnitude because a larger numbers of rooftops corresponding to residential buildings are selected when the threshold of 10–20 degrees tilt is applied.

As can be seen in Table 2, the method presented here for DSP design show that on an hourly basis DSP design could provide a 5% and 9% of net load capacity support per hour in the afternoon and morning times, respectively.

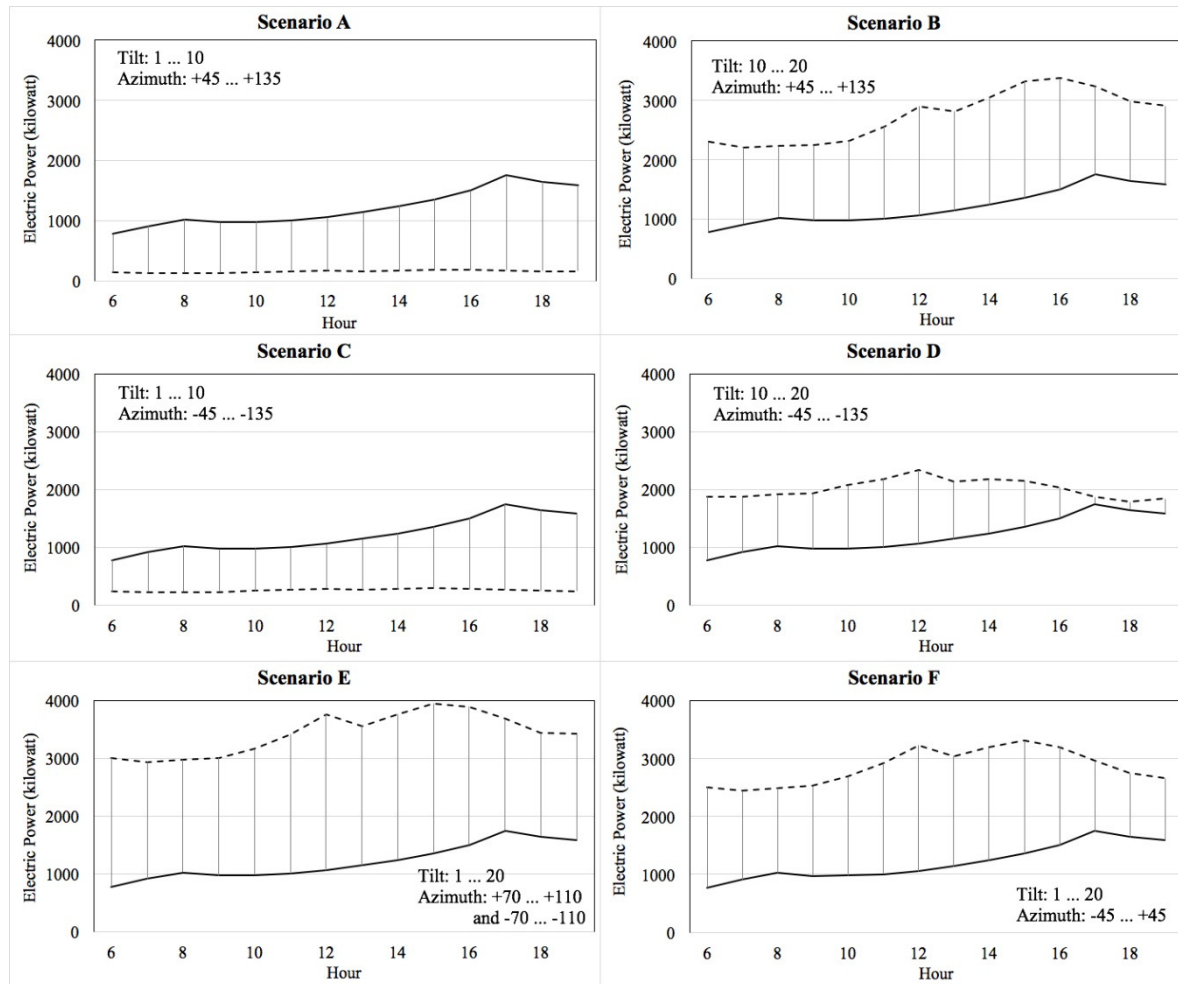


**Figure 13.** Residential Total Load (solid line) and Distributed Solar Plant Generation (dashed line) for 6 scenarios on 21 July.

**Table 2.** Net load capacity support factors for 6 selected scenarios and 4 selected days.

Day	Average Load (KW)	Net Load Capacity Support Factors (%) of Each Scenario					
		A	B	C	D	E	F
21 January	1337	-0.15	-0.36	-0.58	-6.77	-5.02	-3.03
21 April	834	-0.04	3.65	-0.67	-9.20	-3.89	-5.01
21 July	1210	0.29	7.23	0.22	-0.20	5.12	3.27
21 October	1023	0.14	5.22	-0.09	-3.21	1.54	1.06

Similarly, scenarios C and D represent the power profile shape that has a peak during the morning when the facing east rooftop surfaces are selected. Scenario C allows a smaller numbers of commercial buildings' rooftops to be selected with the threshold of 1–10 degrees tilt applied, scenario D allows more rooftops (mostly residential buildings) to be selected with the tilt threshold of 10–20 degrees so the calculated power values in scenario D have larger magnitude. During the summer the solar elevation has a much wider range of 0–84 degrees compared to winter with a range of 0–36, so the morning power generation peak is not as evident in the summer compared to the winter due to the

fact that a large population of rooftop tilt angle in the west-east configuration have steeper tilt angles than 20-degrees. The morning peak is clearly seen in the non-summer months however as evidenced by the controllability factors in Table 2.

Scenarios E and F focus on rooftop surfaces facing south so the differences between morning and afternoon power are not significant among the calculating dates. There are several factors that could determine a value of producing solar power such as different intensities of incident solar irradiances among seasons, the seasonal sun paths or the areas and tilts of surfaces that produce solar power.

Examinations of the six selected scenarios allow us to understand the effects of tilt and azimuth factors on the potential solar energy in one of the LiDAR tiles. It is possible to create a set of rooftop selection criteria within a neighborhood where solar energy produced from those selected surfaces throughout a period of time can meet the expected load—as shown in scenario D when matching load with renewable energy supply in the afternoon.

If a construction developer or designer were to consider this type of analysis/data to apply it to the scale of a neighborhood, they could include this from an urban or suburban planning perspective so that homes orientations and civil road design accounts for a sustainable neighborhood. It is possible in the foreseeable future that urban designers and architects are incentivized to create more sustainable designs that account for DSP to make communities in the aggregate more energy efficient and perhaps obtain tax credits or rebates by the electric utility. Our method presented here adds a perspective to urban/suburban design where construction is done with the electrical grid in mind, as, we would imagine, would be done if a developer has a river going through their construction site and they want to develop their community to meet the supply/demand for water. Only then, we will as a society become truly sustainable, when communities can satisfy their own needs through better collaboration.

The interactions of the solar resource with the general tendencies of urban/suburban planning and the human-built environment are the focus of our study. To assess whether it adds value or not to the utilities, needs would need to be assessed in conjunction with many other factors by utilities and communities (e.g., policies, economic incentives, specific grid design/architecture, building archetypes, climate, demographics, etc.). All of these many variables left out, if added, would make our study much more specific. We have intentionally made it specific to residential communities' characteristics in the Southern United States.

## 5. Conclusions

A systematic quantification approach is adopted in this study to generate rooftop surfaces from LiDAR point clouds and to calculate the potential solar energy from rooftops in San Antonio area. Sets of computer codes are created to automatically process millions of rooftops of every single building in San Antonio, Texas and then to compute central coordinates, area, tilt and azimuth angles of each rooftop. A Python application is developed to calculate the potential hourly solar irradiances and solar energy throughout the year of a neighborhood scale area or a city-wide area. Study results indicate the capabilities of developed computer scripts in accurately processing very large datasets of raw LiDAR data to finally produce useful values of potential solar energy.

The examination of rooftops' geometric characteristics is also performed for the purpose of distributed solar plant (DSP) design at neighborhood scale, with 6 initial selected scenarios that define the rooftop surfaces with up to 20 degrees in tilt angle and various azimuth orientations from facing west and east to facing south. Results indicate different contributions of rooftop's tilt and azimuth angles to the produced daily energy curves, if solar PV panels are installed on these selected rooftops. The method presented here shows that on an hourly basis DSP design and controls could provide a 5% and 9% of controllability to the net load per hour in the afternoon and morning times, respectively.

In a foreseeable future, homes with solar PV will have smart inverters that allow bidirectional communication to control which solar panels on a rooftop are more favorable to the overall condition of the distribution grid. When that time comes, such advanced functionalities will need specific control commands based on inputs from solar forecasting and building assets intelligence. In an effort to

contribute to this discussion, our results show that standard building rooftop tilt angles in the south Texas region has significant impact on the total amount of the energy over the course of a day. Building surfaces' azimuth angle is the most important factor to determine the shape of daily energy profile and its peak location within a day.

This study not only introduces useful computer methods for data processing but also interesting findings that are valuable for the neighborhood scale distributed solar plant (DSP) design and control applications. The methodologies developed in this paper can be employed to study the potential of solar energy in other regions.

**Acknowledgments:** This project and the preparation of this article were funded in part by monies provided by City Public Service (CPS) Energy through an agreement with The University of Texas at San Antonio. We would like to thank the constructional comments from three anonymous reviewers to greatly improve the paper.

**Author Contributions:** Tuan B. Le and Danial Khodli collected and processed the data, analyzed and explained the results. Hongjie Xie and Rolando E. Vega designed the project idea and methodology and guided the data/result interpretation and conclusion development. Bing Dong reviewed the overall building load characterization for estimating energy consumption at the neighborhood scale. Tuan B. Le wrote the paper with help and guidance from co-authors. All co-authors contributed to the paper review and revisions.

**Conflicts of Interest:** The authors declare no conflict of interest.

## References

1. Krayenhoff, E.S.; Voogt, J.A. A microscale three-dimensional urban energy balance model for studying surface temperatures. *Bound. Layer Meteorol.* **2007**, *123*, 433–461. [[CrossRef](#)]
2. Cellura, M.; di Gangi, A.; Longo, S.; Orioli, A. Photovoltaic electricity scenario analysis in urban contests: An Italian case study. *Renew. Sustain. Energy Rev.* **2012**, *16*, 2041–2052. [[CrossRef](#)]
3. Sarralde, J.J.; Quinn, D.J.; Wiesmann, D.; Steemers, K. Solar energy and urban morphology: Scenarios for increasing the renewable energy potential of neighbourhoods in London. *Renew. Energy* **2015**, *73*, 10–17. [[CrossRef](#)]
4. Yu, B.L.; Liu, H.X.; Wu, J.P.; Lin, W.M. Investigating impacts of urban morphology on spatio-temporal variations of solar radiation with airborne LiDAR data and a solar flux model: A case study of downtown Houston. *Int. J. Remote Sens.* **2009**, *30*, 4359–4385. [[CrossRef](#)]
5. Ma, R.J. DEM generation and building detection from LiDAR data. *Photogramm. Eng. Remote Sens.* **2005**, *71*, 847–854. [[CrossRef](#)]
6. Reutebuch, S.E.; Andersen, H.E.; McGaughey, R.J. Light Detection and Ranging (LiDAR): An emerging tool for multiple resource inventory. *J. For.* **2005**, *103*, 286–292.
7. Azizi, Z.; Najafi, A.; Sadeghian, S. Forest road detection using LiDAR data. *J. For. Res.* **2014**, *25*, 975–980. [[CrossRef](#)]
8. Holmgren, J.; Persson, A.; Soderman, U. Species identification of individual trees by combining high resolution LiDAR data with multi-spectral images. *Int. J. Remote Sens.* **2008**, *29*, 1537–1552. [[CrossRef](#)]
9. Liu, C.; Wu, H.; Zhang, Y. Extraction of urban 3D features from LiDAR data fused with aerial images using an improved mean shift algorithm. *Surv. Rev.* **2011**, *43*, 402–414. [[CrossRef](#)]
10. Jiang, J.; Zhang, Z.X.; Ming, Y. Data segmentation for geometric feature extraction from LiDAR point clouds. In Proceedings of the 25th IEEE International Geoscience and Remote Sensing Symposium (IGARSS 2005), Seoul, South Korea, 29–29 July 2005; pp. 3277–3280.
11. Wang, Z.; Wu, L.X. Automated extraction of building geometric features from raw LiDAR data. In Proceedings of the IEEE International Geoscience and Remote Sensing Symposium, Cape Town, South Africa, 12–17 July 2009; pp. 687–690.
12. EXELIS ENVI LiDAR Website. Available online: [http://www.exelisvis.com/docs/using\\_envi\\_lidar\\_Home.html](http://www.exelisvis.com/docs/using_envi_lidar_Home.html) (accessed on 20 January 2015).
13. Masters, G.M. *Renewable and Efficient Electric Power Systems*; John Wiley & Sons Inc.: New York, NY, USA, 2004; Chapter 7.
14. ASHRAE (American Society of Heating, Refrigerating and Air-Conditioning Engineers). Fundamentals: Chapter 14—Climatic Design Information. In *ASHRAE Handbook*; ASHRAE: Atlanta, GA, USA, 2009.

15. Blair, N.; Dobos, A.; Freeman, J.; Neises, T.; Wagner, M.; Ferguson, T.; Gilman, P.; Janzou, S. *System Advisor Model, General Description*; NREL Report No. TP-6A20-61019; NREL: Golden, CO, USA, 2014; p. 19.
16. Gueymard, C.A. REST2: High-performance solar radiation model for cloudless-sky irradiance, illuminance, and photosynthetically active radiation—Validation with a benchmark dataset. *Sol. Energy* **2008**, *82*, 272–285. [[CrossRef](#)]
17. Ames, D.P.; Pinthong, K.; Scott, M.; Khattar, R.; Solan, D.; Lee, R. Open source map based software for photovoltaic system layout design. In Proceedings of the 7th International Congress on Environmental Modeling and Software—International Environmental Modeling and Software Society (iEMSs), San Diego, CA, USA, 15–19 June 2014.
18. Reda, I.; Andreas, A. Solar position algorithm for solar radiation applications. *Sol. Energy* **2004**, *76*, 577–589. [[CrossRef](#)]
19. Joudi, K.A.; Al-tabbakh, A.A. Computer simulation of a two phase thermosyphon solar domestic hot water heating system. *Energy Convers. Manag.* **1994**, *40*, 775–793. [[CrossRef](#)]
20. Al-Sanea, S.A.; Zedan, M.F.; Al-Ajlan, S.A. Adjustment afctors for the ASHRAE clear-sky model based on solar-radiation measurements in Riyadh. *Appl. Energy* **2004**, *79*, 215–237. [[CrossRef](#)]
21. Gueymard, C.A.; Thevenard, D. Monthly average clear-sky broadband irradiance database for worldwide solar heat gain and building cooling load calculations. *Sol. Energy* **2009**, *83*, 1998–2018. [[CrossRef](#)]
22. Hassouneh, K.; Alshboul, A.; Al-Salaymeh, A. Influence of windows on the energy balance of apartment buildings in Amman. *Energy Convers. Manag.* **2010**, *51*, 1583–1591. [[CrossRef](#)]
23. Jin, F.; Chen, Z.; Wang, J.T.; Yang, J. Practical procedure of predicting non-uniform temperature on the exposed face of arch dams. *Appl. Therm. Eng.* **2010**, *30*, 2146–2156. [[CrossRef](#)]
24. Gueymard, C.A. Impact of on-site atmospheric water vapor estimation methods on the accuracy of local solar irradiance predictions. *Sol. Energy* **2014**, *101*, 74–82. [[CrossRef](#)]
25. Dewberry. *LiDAR Quality Assurance (QA) Report*; Bexar County—Texas Water Development Board: San Antonio, TX, USA, 2011.
26. Gatziolis, D.; Andersen, H.E. *A Guide to LiDAR Data Acquisition and Processing for the Forests of the Pacific Northwest*; United States Department of Agriculture: Portland, OR, USA, 2008.
27. Cheuk, M.L.; Yuan, M. Assessing spatial uncertainty of LiDAR-derived building model: A case study in downtown Oklahoma City. *Photogramm. Eng. Remote Sens.* **2009**, *74*, 257–269. [[CrossRef](#)]
28. Labiak, R.C.; van Aardt, J.A.N.; Bespalov, D.; Eychner, D.; Wirch, E.; Bischof, H.P. Automated method for detection and quantification of building damage and debris using post-disaster LiDAR data. *Proc. SPIE* **2011**. [[CrossRef](#)]
29. Hermosilla, T.; Ruiz, L.A.; Recio, J.A.; Estornell, J. Evaluation of automatic building detection approaches combining high resolution images and LiDAR data. *Remote Sens.* **2011**, *3*, 1188–1210. [[CrossRef](#)]
30. Kim, S.; McGaughey, R.J.; Andersen, H.E.; Schreuder, G. Tree species differentiation using intensity data derived from leaf-on and leaf-off airborne laser scanner data. *Remote Sens. Environ.* **2009**, *113*, 1575–1586. [[CrossRef](#)]
31. Maas, H.G.; Vosselman, G. Two algorithms for extracting building models from raw laser altimetry data. *ISPRS J. Photogramm. Remote Sens.* **1999**, *54*, 153–163. [[CrossRef](#)]
32. Tarsha-Kurdi, F.; Landes, T.; Grussenmeyer, P.; Koehl, M. Model-driven and data-driven approaches using LiDAR data: Analysis and comparison. *Int. Arch. Photogramm. Remote Sens. Spat. Inf. Sci.* **2007**, *36*, 87–92.
33. Jochem, A.; Höfle, B.; Rutzinger, M.; Pfeifer, N. Automatic roof plane detection and analysis in airborne lidar point clouds for solar potential assessment. *Sensors* **2009**, *9*, 5241–5262. [[CrossRef](#)] [[PubMed](#)]
34. Vittal, P.R. *Analytical Geometry: 2D and 3D*; Pearson: New Delhi, India, 2013; p. 752.
35. ERCOT. *Report on the Capacity, Demand, and Reserves in the ERCOT Region, 2015–2024*; ERCOT: Austin, TX, USA, 2014.
36. Szabo, S.; Enyedi, P.; Horvath, M.; Kovacs, Z.; Burai, P.; Csoknyai, T.; Szabo, G. Automated registration of potential locations for solar energy production with Light Detection And Ranging (LiDAR) and small format photogrammetry. *J. Clean. Product.* **2016**, *112*, 3820–3829. [[CrossRef](#)]
37. Lukac, N.; Zlaus, D.; Seme, S.; Zalik, B.; Stumberger, G. Rating of roofs' surfaces regarding their solar potential and suitability for PV systems, based on LiDAR data. *Appl. Energy* **2013**, *102*, 803–812. [[CrossRef](#)]

38. Huang, Y.; Chen, Z.; Wu, B.; Chen, L.; Mao, W.; Zhao, F.; Wu, J.; Wu, J.; Yu, B. Estimating roof solar energy potential in the downtown area using a GPU-accelerated solar radiation model and airborne LiDAR data. *Remote Sens.* **2015**, *7*, 17212–17233. [[CrossRef](#)]
39. Dobos, A.P. *PVWatts Version 5 Manual*; Technical Report NREL/TP-6A20-62641; NREL: Golden, CO, USA, 2014; p. 16.



© 2016 by the authors; licensee MDPI, Basel, Switzerland. This article is an open access article distributed under the terms and conditions of the Creative Commons by Attribution (CC-BY) license (<http://creativecommons.org/licenses/by/4.0/>).